Shrinkage cracks of bentonite-zeolite mixtures

Yew-Heng Sherman Seah[1] and *Eng-Choon* Leong[1*]

[1]Nanyang Technological University, School of Civil and Environmental Engineering, 50 Nanyang Avenue, 639798, Singapore

Abstract. Bentonite is commonly used in geosynthetic clay liner (GCL) as well as compacted clay liner (CCL) for containment facilities such as sanitary landfills due to its low permeability. Bentonite experiences significant shrinkage on drying, leading to the formation of desiccation cracks and increasing the likelihood of contaminant leachate from the landfill. Adding granular materials such as fine sand to bentonite can reduce shrinkage and hence shrinkage cracks. Recently, zeolite has been suggested as another possible additive to reduce be shrinkage cracks in bentonite. Zeolite has additional benefits of being able to adsorb heavy metals and when enriched with silver, zinc, or copper, it can function as a biocide. The objective of this paper is to present the results of a study on shrinkage crack formation of bentonite-zeolite mixtures during drying. The evolution of shrinkage cracks of the bentonite-zeolite mixtures on drying was studied using image processing. The results show that desiccation cracks are at a minimum when the zeolite content is between 15% and 20%. The finding is useful to design more efficient GCL or CCL when zeolite is incorporated into the bentonite layer.

1 Introduction

Bentonite is commonly used in geosynthetic clay liner (GCL) as well as compacted clay liner (CCL) for sanitary landfills due to its low permeability. A common problem with bentonite is bentonite experiences significant shrinkage on drying resulting in formation of desiccation cracks [1-5] and increasing its permeability to allow leachate from the landfill to seep through the GCL or CCL and contaminates the surrounding environment. Therefore, additional material has been added to bentonite to reduce the likelihood of shrinkage and formation of shrinkage cracks.

Bentonite-sand mixtures have been proposed for GCL to solve the shrinkage cracks problem. Kleppe and Olson concluded that when bentonite is mixed with coarser particles shrink-swell and/or freeze-thaw cycling cracks are eliminated using bentonite-sand mixtures [6]. Recently, zeolite has been proposed as an alternative to sand [7-10]. Zeolites are a family of hydrated aluminosilicate minerals containing alkali and alkaline-earth metals. Besides occurring naturally, zeolites can be synthesized from fly ash, a by-product from coal combustion [11, 12]. Since fly ash typically ends up in a sanitary landfill, converting the fly ash to zeolite and using it in GCL and CCL is attractive.

Zeolites have cation-exchange property [13] and can absorb heavy metals and function as a biocide when enriched with silver, zinc, or copper. This makes zeolite more attractive than sand to reduce the shrinkage problem in bentonite.

The objective of this study is to investigate the development of shrinkage cracks in bentonite-zeolite mixtures of different proportions and to determine the optimum mixture at which shrinkage cracks are at a minimum.

2 Materials and methods

2.1 Materials

The materials that are used in the experiments are bentonite and zeolite. Both materials are procured from commercial sources. The bentonite used is fine-grained with 100 % passing through a 0.075 mm (No. 200) sieve. The zeolite (Z4) used is coarse-grained and uniform with particle sizes between 1.0 and 2.0 mm. The properties of bentonite and zeolite are summarised in Table 1.

2.2 Methods

2.2.1 Sample preparation

The samples were prepared using oedometer apparatus following ASTM D2435-11 for oedometer test [14]. Dry bentonite and zeolite were taken from their original packaging and mixed manually in a bowl such that the weight for each sample was fixed at 76 g. The mixture was separated into two equal portions. One portion was transferred into the oedometer load ring cell and statically compacted to the halfway mark. The surface of the compacted layer was then scored, and the second

---

* Corresponding author: cecleong@ntu.edu.sg

portion was added and compacted such that it filled the oedometer load ring cell. A piece of wetted filter paper was placed on the saturated porous stone, followed by the sample in the oedometer ring and then another piece of wetted filter paper was placed on top of the sample. After assembling the oedometer setup, a vertical pressure of 120 kPa was applied to simulate k_0 loading of a GCL or CCL in a landfill. The oedometer cell was then inundated with water to allow the mixture to saturate and swell in a controlled manner.

The sample was removed from the oedometer apparatus after 24 hours. The weight and dimensions of the samples were then recorded. Each sample was also checked to ensure that there were no cracks or fissures in the sample.

Bentonite-zeolite samples of 5% to 30% zeolite content by dry weight were prepared using the above procedures. The samples were denoted as Z5, Z10, Z15, Z20, Z25 and Z30 for zeolite contents of 5%, 10%, 15%, 20%, 25% and 30%, respectively. Sample of 100% bentonite is used as a control and it is denoted as Z0.

Table 1. Basic properties of bentonite and zeolite used in study

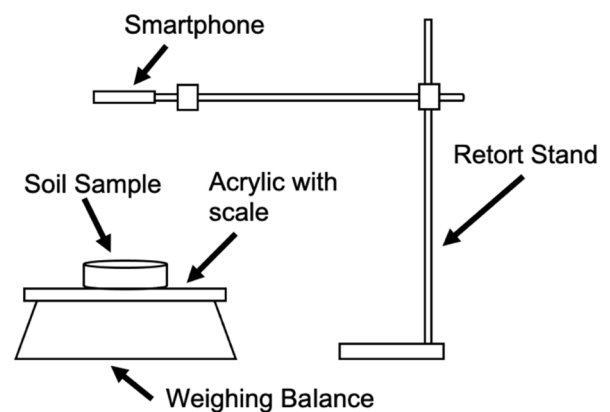| Bentonite		Zeolite	
Parameter	Value	Parameter	Value
Moisture (% by wt)	13.4	Size < 1 mm (% by wt)	0.2
pH	10-11	Size > 2 mm (% by wt)	1.9
Free swelling (Ml)	31	Crush strength, Schleuniger (N)	22
Liquid limit (%)	534	Tapped bulk density EN ISO 787-11 (g/l)	711
Molecular weight	180.06	Water adsorption, 50%rH, 20°C, 24 hours (% by wt)	21
Sp. gravity	2.77	Sp. gravity	2.26

2.2.2 Pressure plate test

Controlled drying of the bentonite-zeolite samples were done using pressure plates (ASTM D6836 – 16, 2016, Method C) [15]. A 5-bar pressure plate was used for matric suction up to 500 kPa and a 15-bar pressure plate was used for matric suction up to 1000 kPa. The high-air entry ceramic disks of the pressure plates were saturated with distilled water before use.

The samples were placed in the 5-bar pressure plate and matric suctions of 120 kPa, 200 kPa, and 400 kPa were applied. After attaining equilibrium at 400 kPa in the 5-bar pressure plate, the samples were transferred to the 15-bar pressure plate and matric suction of 700 kPa and 900 kPa were applied. Suction equilibrium of the samples was determined by weighing the samples

periodically at each applied matric suction until the change in weight of the sample was negligible.

At suction equilibrium, the samples were photographed using the set-up shown in Fig. 1. The weight change and matric suction also enables the SWCC of the bentonite-zeolite mixture to be determined.

Fig. 1. Schematic of set-up for photographing bentonite-zeolite samples.

2.2.3 WP4 Dew Point Potentiometer Test

To complete the SWCC of the bentonite-zeolite samples, the WP4 Dew Point Potentiometer was used to measure the matric suction of a small piece of the sample (ASTM D6836 – 16, 2016, Method D) [15].

The sub-samples were placed in WP4 sample cups and left in an open container to dry under ambient condition. Suctions and weight of the sub-samples were measured every few days.

3 Results and discussion

3.1 Soil-water characteristic curve

The soil-water characteristic curves (SWCCs) of the bentonite-zeolite samples are summarised in Fig. 2. The water content of the SWCC is given in terms of gravimetric water content. Fig. 2 shows that the shapes of the SWCCs of the bentonite-zeolite samples are similar regardless of the zeolite content implying that their hydraulic properties are largely similar.

3.2 Shrinkage

The development of cracks in the physical samples on drying are only shown for in Fig. 2. Samples Z0, Z5, and Z10 showed the most severe desiccation cracks. The severity of the cracks decreases drastically as zeolite content increases to 15% (Z15) and 20% (Z20) and thereafter, the cracks start to increase again for Z25 and Z30.

Ören et al. [16] suggested that zeolite and bentonite particles compete for water in a bentonite-zeolite mixture. Zeolite grains have a greater tendency than bentonite to absorb water based on three factors: The

porosity of the structure, the rough surface, and the lower water entry pressure [16]. Hence, on drying the water in the zeolite particles is slowly pulled away by the bentonite, reducing the propensity for crack to form in the bentonite-zeolite mixture.

To quantify the extent of the cracks for the bentonite-zeolite samples, a mechanical descriptor is more useful. Mi and Miller et al. proposed Crack-Intensity-Factor (CIF) as a descriptor for surface cracks [17, 18]. The CIF is defined as the time-variable ratio of surface crack area, A_c, to the total surface area of the clay, A_t. In order, to determine the surface crack areas, an image processing tool for the photographs of the samples is needed. This is explained in the next section.
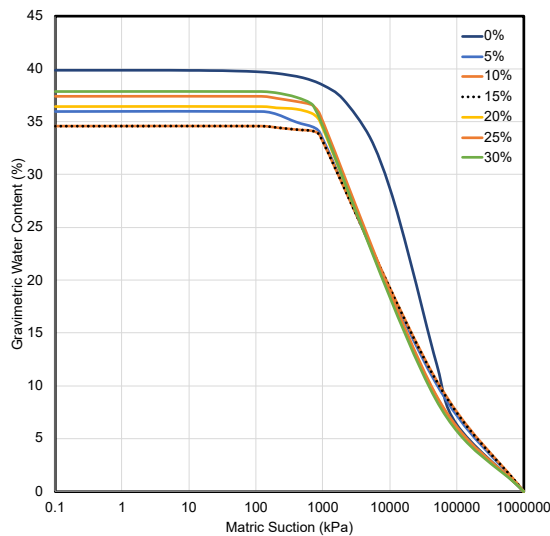
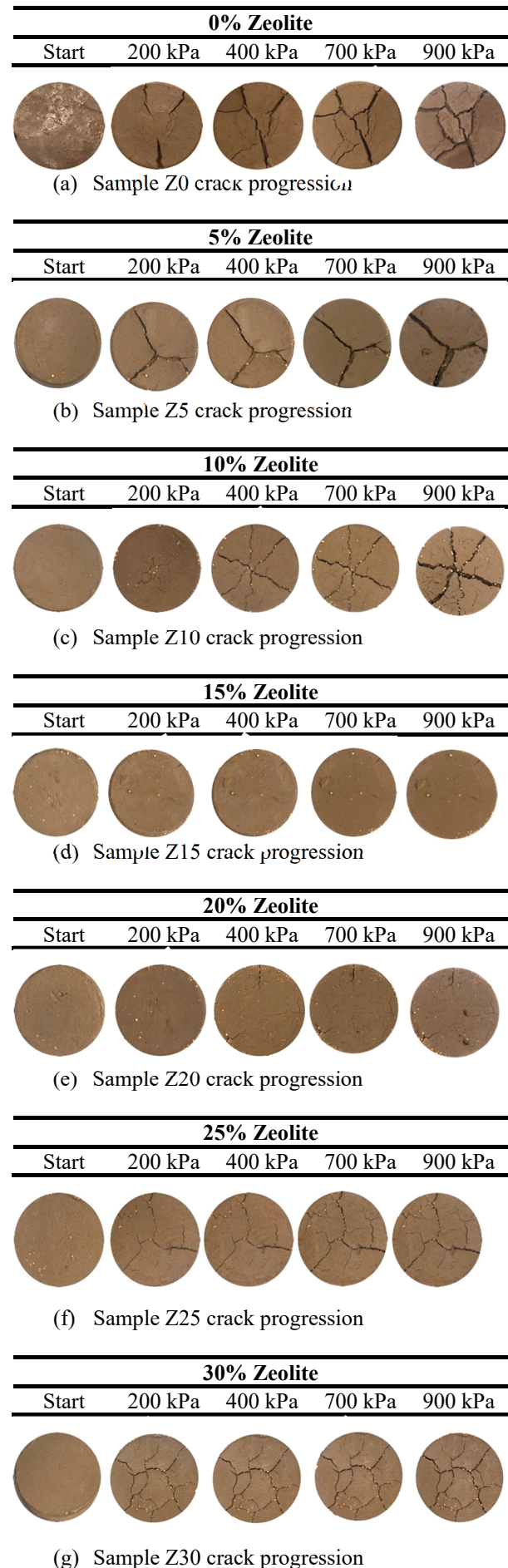**Fig. 2.** SWCCs for all bentonite-zeolite samples

3.3 ImageJ

Image analysis methodology in the determination and quantification of cracks by using computer software has been gaining traction in the past few decades [18-22].

ImageJ has been widely adopted in the field of immunohistochemistry (IHC) to quantify stained tissues. ImageJ is ideal for this study because of its accessibility as it is open-source and is freely available across various operating systems. ImageJ also does not require computers with high computational power or coding experiences from the user [23-27].

In this paper, the development of cracks was investigated with ImageJ and the steps adopted to quantify the cracks are similar to the method adopted in the imaging for IHC [26, 27]. The background in the photographs of the bentonite-zeolite samples were first removed. The images were then converted into an RBG stack. A montage was created based on the RBG stack.

A contrast "threshold" was set such that the cracks become highly visible. A "measure" function was used to obtain the percentage of the surface area that was coloured red representing the uncracked surface area A_{uc} of the bentonite-zeolite sample. Subtracting the A_{uc} from the total surface area A_t gives the cracked surface area A_c and hence, CIF is determined by taking the ratio of A_c to A_t. The procedures are illustrated in Table 2.

(a) Sample Z0 crack progression

(b) Sample Z5 crack progression

(c) Sample Z10 crack progression

(d) Sample Z15 crack progression

(e) Sample Z20 crack progression

(f) Sample Z25 crack progression

(g) Sample Z30 crack progression

Fig. 3. Crack development in bentonite-zeolite samples

Table 2. Steps for ImageJ quantification of cracks in bentonite-zeolite samples.

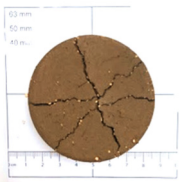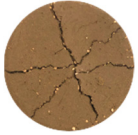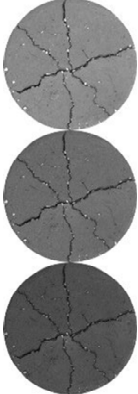| No.	Steps	Corresponding Image
1	Photograph of the sample was taken.	
2	Background of sample image was removed.	
3	Image was converted into an RGB stack, and the red layer was selected.	
4	Contrast threshold was set such that the cracks become highly visible.	
5	The "measure" function was used to obtain the uncracked surface area A_{uc}. The uncracked and total surface areas A_t were used to determine CIF.	$A_c = A_t - A_{uc}$ $CIF = A_c/A_t$

Table 3 shows a summary of the calculated CIFs of the various bentonite-zeolite samples at suctions of 120 kPa. 200 kPa, 400 kPa, 700 kPa and 900 kPa. The CIFs presented in Table 2 is expressed in percentage.

Fig. 4 shows a plot of the CIFs of the various bentonite-zeolite samples at a suction of 900 kPa. Fig. 4 shows that as the zeolite content increases from 0% to 15%, the CIF decreases, showing a reduction of desiccation cracks. However, when the zeolite content increases beyond 15%, the CIF increases again. This can be attributed to the larger number of zeolite particles present in the bentonite-zeolite sample providing sites for crack initiations during drying.

Fig. 5 shows the evolution of CIF for the various bentonite-zeolite samples. For the samples with low zeolite content (Z0, Z5 and Z10), CIF is seen to increase rapidly between suctions of 700 kPa and 900 kPa, whereas samples with higher zeolite content (Z15, Z20, Z25 and Z30) shows that the CIF plateaued after suction of 400 kPa. This suggest that higher zeolite content is beneficial in reducing desiccation cracks.

From Figs. 4 and 5, it can be concluded that the optimum zeolite content for minimum desiccation cracks in bentonite-zeolite mixtures is between 15% and 20%.

Table 3. Evolution of CIF (%) of bentonite-zeolite samples

Sample ID	Suction (kPa)				
	120	200	400	700	900
Z0	0	5.852	8.592	9.534	10.819
Z5	0.605	5.703	7.327	7.557	10.418
Z10	0.214	1.900	6.641	7.128	8.867
Z15	0.090	0.651	2.429	2.552	2.602
Z20	0.396	0.765	2.838	3.010	3.067
Z25	0.592	3.144	4.565	4.874	5.094
Z30	0.933	2.848	4.770	5.410	5.544
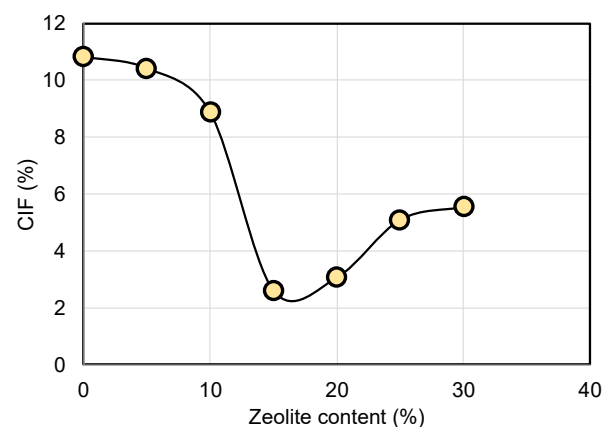
Fig. 4. Plot of CIF (%) versus zeolite content (%) at suction of 900kPa.

4 Conclusion and future works

4.1 Conclusion

The development of shrinkage cracks in bentonite-zeolite mixtures was investigated in this study for zeolite contents ranging from 0% to 30%. The bentonite-zeolite samples were prepared by static compaction, loaded under k_0 loading condition of 120 kPa and inundated. The samples were then removed and placed in the pressure plate for controlled drying at various matric

suctions. Hence, the soil-water characteristic curves (SWCCs) of the bentonite-zeolite samples were also obtained. The soil-water characteristics of the sample at suctions higher than 1000 kPa were obtained using the WP4. Photographs of the bentonite-zeolite samples were taken at each suction equilibrium. The surface cracks of the bentonite-zeolite samples were quantified using CIF. The SWCCs of the bentonite-zeolite samples are similar regardless of zeolite content indicating that the hydraulic properties remain largely similar. The CIF showed that the desiccation cracks of the bentonite-zeolite samples were minimum when zeolite content was between 15% and 20%.

4.2 Future works

There are several areas of this study that can be improved:

First, the bentonite-zeolite samples were prepared by static compression and saturated under k_0 loading condition at 120 kPa. The effect of the sample preparation may affect the CIF observations. Hence, effect of sample preparation on crack development needs to be further investigated.

Second, an artificial zeolite Z4 with particle sizes between 1 and 2 mm was used in this study. There are more than 150 types of artificial zeolites. Other zeolites should be used to investigate if the results obtained in this study can be extrapolated to other zeolites.

Third, for bentonite-zeolite mixture to be used in CCL and GCL, its hydraulic conductivity should be less than $1e^{-9}$ m/s and $5e^{-11}$ m/s, respectively, under the environmental guidelines for solid waste landfills published by the Environment Protection Authority (EPA), New South Wales, Australia [28]. Hydraulic conductivity of the bentonite-zeolite mixtures was not determined in this study.

Lastly, the efficacy of zeolite in removing heavy metals and other contaminants within the bentonite has yet to be investigated.
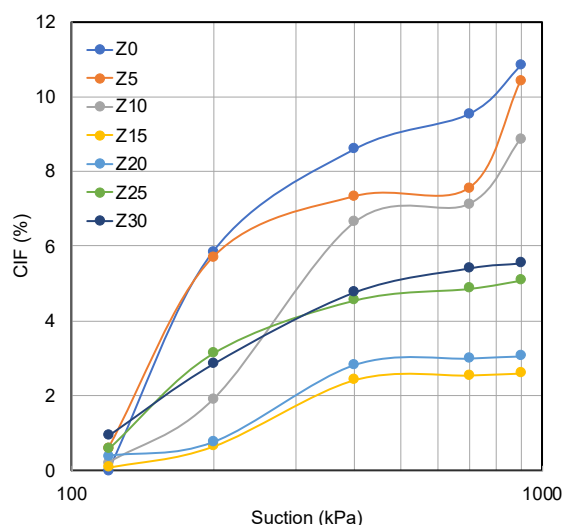

Fig. 5. Plot of CIF (%) versus suction (kPa)

References

1. W. S. Abdullah, K. A. Alshibli, and M. S. Al-Zou'bi, Appl. Clay Sci., **15**, 447–462 (1999)
2. C. H. Benson and M. A. Othman, J. Geo. Eng., **119**, 276–294 (1993)
3. C. H. Benson, T. H. Abichou, M. A. Olson, and P. J. Bosscher, J. Geo. Eng., **121,** 69–79 (1995)
4. H. Komine and N. Ogata, Can. Geo. J., **31**, 478–490 (1994)
5. M. A. Othman, C. H. Benson, E. J. Chamberlain, and T. F. Zimmie, Hydr. Cond. And Wast. Cont. Tran. In Soil, **142**, 227-227–28 (2009)
6. J. H. Kleppe and R. E. Olson, in Hydr. Barr. In Soil and Rock, **874**, 263-263–13 (1985)
7. A. Z. Woinarski, G. W. Stevens, and I. Snape, Proc. Saf. Envi. Prot., **84**, 109–116 (2006)
8. A. Kaya and S. Durukan, Appl. Clay Sci., **27**, 241 (2004)
9. K. Kayabali, Eng. Geol., **46**,105–114 (1997)
10. A. Tuncan, M. Tuncan, H. Koyuncu, and Y. Guney, Waste Manag. Res., **21**, 54–61 (2003)
11. V. Somerset, L. Petrik, and E. Iwuoha, J. Envi. Mana., **87**, 125–131 (2008)
12. L. F. Petrik, V. R. K. Vadapalli, W. M. Gitari, A. Ellendt, and G. Balfour, S. Afr. J. Sci., **106** (2010)
13. S. M. Auerbach, K. A. Carrado, and P. K. Dutta, Hand. Of zeol. Sci. and tech. (2003)
14. ASTM Standard D2435-11 (2012)
15. ASTM Standard D6836-16 (2016)
16. A. H. Ören, A. Kaya, and A. Ş. Kayalar, Can. Geotech. J., **48**, 1343–1353 (2011)
17. Mi, H., Ph.D. Thes., Dep. Of Civil and Envi. Engi. (1995)
18. Miller, C.J., Mi, H., Yesiller, N., J. Am. Water Resou. Assoc., **34**, 677–686. (1998)
19. Velde, B., Geod., **93**, 101–112 (1999)
20. Yan, A., Wu, K., Zhang, X., Cem. Concr. Res., **32**, 1371–1375 (2002)
21. Yesiller, N., Miller, C.J., Inci, G., Yaldo, K., Eng. Geol., **57**, 105–121 (2002)
22. C.S. Tang, B. Shi, C. Liu, L.Z. Zhao, B.J. Wang, Eng. Geo., **101**, 204-217 (2008)
23. Crowe, A. R., & Yue, W, Bio-Protocol, **9** (2019)
24. Young, K., & Morrison, H. Jour. Of Vis. Exp.: JoVE, **136**, (2018).
25. Vrekoussis, T., Chaniotis, V., Navrozoglou, I., Dousias, V., Pavlakis, K., Stathopoulos, E. N., & Zoras, O., Anti. Res., **29**, 4995-4998 (2009)
26. G. Jian, S. Peng, X. Shan, G.L. Deng, L.H. Sheng, J. Sun, C.H. Jiang, **10**, 957 (2019)
27. L. Liya, W.J. Liu, H. Wang, Q.J. Yang, L.Q. Zhang, F. Jin, Y. Jin, **9**, 1-11 (2018)
28. EPA, Guidelines [Online] (2016), https://www.epa.nsw.gov.au/publications/waste/ solid-waste-landfill-guidelines-160259. [Accessed: 25-Apr-2022].